Chinese Journal of Aeronautics 24 (2011) 434-448

Contents lists available at ScienceDirect

Chinese Journal of Aeronautics

journal homepage: www.elsevier.com/locate/cja

Static Analysis of Functionally Graded Sandwich Plates Using an Efficient and Simple Refined Theory

Hadj Henni ABDELAZIZ[a,b], Hassen Ait ATMANE[a,c], Ismail MECHAB[a], Lakhdar BOUMIA[d], Abdelouahed TOUNSI[a,*], Adda Bedia El ABBAS[a]

[a]*Laboratoire des Matériaux et Hydrologie, Université de Sidi Bel Abbes, BP 89 Cité Ben M'hidi, Sidi Bel Abbes 22000, Algérie*

[b]*Département de Génie Civil, Université Ibn Khaldoun, BP 78 Zaaroura, Tiaret 14000, Algérie*

[c]*Département de Génie Civil, Faculté de Génie Civil et d'Architecture, Univesité de Chlef, Chelf 20000, Algérie*

[d] *Département de Physique, Université de Sidi Bel Abbes, BP 89 Cité Ben M'hidi, Sidi Bel Abbes 22000, Algérie*

Received 13 December 2010; revised 6 February 2011; accepted 12 April 2011

Abstract

In this paper, a new displacement based high-order shear deformation theory is introduced for the static response of functionally graded sandwich plate. Unlike any other theory, the number of unknown functions involved is only four, as against five in case of other shear deformation theories. The theory presented is variationally consistent, has strong similarity with classical plate theory in many aspects, does not require shear correction factor, and gives rise to transverse shear stress variation such that the transverse shear stresses vary parabolically across the thickness satisfying shear stress free surface conditions. Two common types of functionally graded sandwich plates, namely, the sandwich with functionally graded facesheet and homogeneous core and the sandwich with homogeneous facesheet and functionally graded core, are considered. Governing equations are derived from the principle of virtual displacements. The closed-form solution of a simply supported rectangular plate subjected to sinusoidal loading has been obtained by using the Navier method. The validity of the present theory is investigated by comparing some of the present results with those of the classical, the first-order and the other higher-order theories. It can be concluded that the proposed theory is accurate and simple in solving the static bending behavior of functionally graded sandwich plates.

Keywords: functionally graded materials; sandwich plates; refined plate theory; bending; Navier solution

1. Introduction

Functionally graded materials (FGMs) are new inhomogeneous materials which have been widely used in many engineering applicants such as nuclear reactors and high-speed spacecraft industries [1]. The mechanical properties of FGMs vary smoothly and continuously from one surface to the other. Typically these materials are made from a mixture of ceramic and metal or from a combination of different materials. The ceramic constituent of the material provides the high-temperature resistance due to its low thermal conductivity. The ductile metal constituent on the other hand, prevents fracture caused by stresses due to the high temperature gradient in a very short period of time. Furthermore a mixture of ceramic and metal with a continuously varying volume fraction can be easily manufactured [2-3]. With the developments in manufacturing methods [2,4-7] FGMs seem to have great potential in sandwich structures. The analysis of these materials has been considered by many researchers.

*Corresponding author. Tel.: +213-48-564100.
E-mail address: tou_abdel@yahoo.com

doi: 10.1016/S1000-9361(11)60051-4

A considerable amount of literature exists on sandwich plates as they are used in large number of applications varying from high-performance composites in aerospace structures to low-cost materials for building constructions. The limitations of classical plate theory in describing complex problems (e.g., contact/impact problems, behavior of thick laminate plates) necessitated the development of higher-order theories. The term "higher-order" refers to the level of truncation of terms in a power series expansion of displacements about the thickness coordinate. Reissner [8] and Midlin [9] were the first to propose a plate theory that included the effect of shear deformation and that assumed linear longitudinal displacements and constant transverse displacements. Midlin [9] introduced the correction factor into the shear stress to account for the fact that the model predicts a uniform shear stress through the thickness of the plate. Yang, et al. [10] extended Midlin's theory for homogeneous plates to laminates consisting of arbitrary number of bonded layers. Based on the same model (Midlin's theory), Whitney and Pagano [11] developed a theory for anisotropic laminated plates consisting of an arbitrary number of bonded anisotropic layers that includes shear deformation and rotary inertia. Displacement field is assumed to be linear in thickness coordinate. Since then, the plate theory was improved by including higher-order terms in displacement assumptions. Essenburg [12] assumed second-order transverse displacements and linear longitudinal displacements; Reissner [13] included third-order terms in the in-plane displacements' z-expansion; Lo, et al. [14-15] included third-order in-plane and second-order out-of-plane terms. Reddy [16] developed a third-order shear deformation plate theory (TSDPT) for composite laminates, based on assumed displacement fields (third-order in-plane and constant out-of-plane displacements).

The FGM sandwich plate can alleviate the large interfacial shear stress concentration because of the gradual variation of material properties at the facesheet-core interface. The effects of FGM core were studied by Venkataraman and Sankar [17], and Anderson [18] on the shear stresses at the facesheet-core of FGM sandwich beam. Pan and Han [19] analyzed the static response of the multilayered rectangular plate made of functionally graded, anisotropic and linear magneto-electro-elastic materials. Das, et al. [20] studied a sandwich composed of a single FGM soft core with relatively orthotropic stiff facesheets by using a triangular plate element. Shen [21] considered two types of FGM hybrid laminated plates, one is with FGM core and piezoelectric ceramic facesheet and the other is with FGM facesheet and piezoelectric ceramic core.

The FGM sandwich construction commonly exists in two types: FGM facesheet-homogeneous core and homogeneous facesheet-FGM core. For the case of homogeneous core, the softcore is commonly employed because of the light weight and high bending stiffness in the structural design. The homogeneous hardcore is also employed in other fields such as control or in the thermal environments. The actuators and sensors which are commonly piezoelectric ceramics are always in the mid layers of the sandwich construction as in the paper of Shen [21]. Moreover, in the thermal environments, the metal-rich facesheet can reduce the large tensile stress on the surface at the early stage of cooling [22].

As far as we know, there has been no investigation on bending response of FGM sandwich plates using two variable refined plate theory (RPT). This theory was developed by Shimpi [23] for isotropic plates, and was extended by Shimpi and Patel [24-25] for orthotropic plates. The most interesting feature of this theory is that it does not require shear correction factor, and has strong similarities with the classical plate theory (CPT) in some aspects such as governing equation, boundary conditions and moment expressions.

The purpose of this paper is to extend the RPT developed by Shimpi and Patel [24-25] to the static response of FGM sandwich plates. The present theory satisfies equilibrium conditions at the top and bottom faces of the sandwich plate without using shear correction factors. Navier solution is used to obtain the closed-form solutions for simply supported FGM sandwich plates. Numerical examples are presented to illustrate the accuracy and efficiency of the present theory in predicting the stresses and displacements of FGM sandwich plates by comparing the predictions with those computed using various theories.

2. RPT for FGM Sandwich Plates

2.1. Geometrical configuration

Consider the case of a uniform thickness, rectangular FGM sandwich plate composed of three microscopically heterogeneous layers referring to rectangular coordinates (x, y, z) as shown in Fig. 1. The top and bottom faces of the plate are at $z=\pm h/2$, and the edges of the plate are parallel to axes x and y. The two side lengthes are a and b.

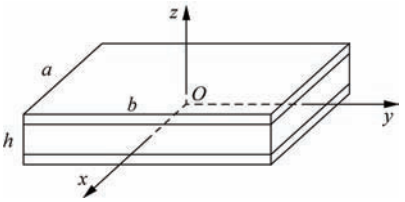

Fig. 1 Geometry of rectangular FGM sandwich plate with uniform thickness in rectangular Cartesian coordinates.

The sandwich plate is composed of three elastic layers, namely, Layer 1, Layer 2, and Layer 3 from bottom to top of the plate. The vertical ordinates of the bottom, the two interfaces, and the top are denoted by $h_1=-h/2$, h_2, h_3, $h_4=h/2$, respectively. For the brevity, the ratio of the thickness of each layer from bottom to top is denoted by the combination of three numbers,

i.e. 1-0-1, 2-1-2 and so on. As shown in Fig. 2, two types, Type A and Type B are considered in the present study:

Type A—FGM facesheet and homogeneous core.

Type B—Homogeneous facesheet and FGM core.

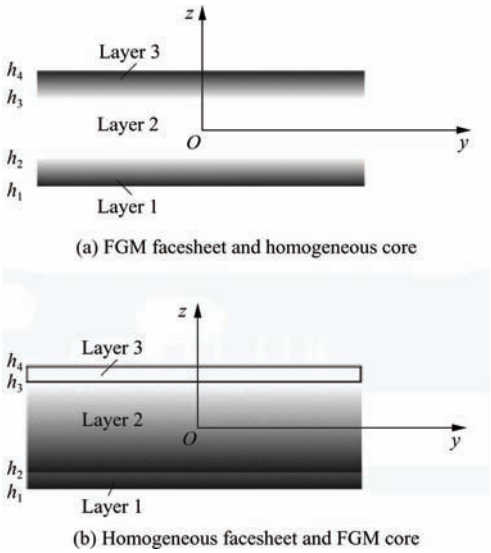

Fig.2 Material variation along the thickness of FGM sandwich plate.

2.2. Material properties

The properties of FGM vary continuously due to the gradual change in the volume fraction of the constituent materials, usually in the thickness direction only. Power-law function is commonly used to describe these variations of material properties. The sandwich structures made of two types of power-law FGMs mentioned before are discussed as follows.

2.2.1. Type A—power-law FGM facesheet and homogeneous core

The volume fraction of the FGMs is assumed to obey a power-law function along the thickness direction:

$$\begin{cases} V^{(1)} = \left(\dfrac{z-h_1}{h_2-h_1}\right)^k & z\in[h_1,h_2] \\ V^{(2)} = 1 & z\in[h_2,h_3] \\ V^{(3)} = \left(\dfrac{z-h_4}{h_3-h_4}\right)^k & z\in[h_3,h_4] \end{cases} \tag{1}$$

where $V^{(n)}$ (n=1, 2, 3) denotes the volume fraction function of Layer n; k the volume fraction index ($0\le k\le+\infty$), which dictates the material variation profile through the thickness.

2.2.2. Type B—homogeneous facesheet and power-law FGM core

The volume fraction of the FGMs is assumed to obey a power-law function along the thickness direction:

$$\begin{cases} V^{(1)} = 0 & z\in[h_1,h_2] \\ V^{(2)} = \left(\dfrac{z-h_2}{h_3-h_2}\right)^k & z\in[h_2,h_3] \\ V^{(3)} = 1 & z\in[h_3,h_4] \end{cases} \tag{2}$$

The effective material properties, like elastic modulus E and Poisson's ratio ν, then can be expressed by the rule of mixture [26] as

$$P^{(n)}(z) = P_2 + (P_1 - P_2)V^{(n)} \tag{3}$$

where $P^{(n)}$ is the effective material property of FGM of Layer n. For Type A, P_1 and P_2 are the properties of the top and bottom faces of Layer 1, respectively, and vice versa for Layer 3 depending on the volume fraction $V^{(n)}$(n=1, 2, 3). For Type B, P_1 and P_2 are the properties of Layer 3 and Layer 1, respectively.

These two types of FGM sandwich plates will be discussed later in the following sections. For simplicity, Poisson's ratio of plate is assumed to be constant in this study for that the effect of Poisson's ratio on the deformation is much less than that of elastic modulus [27].

2.3. Basic assumptions

Assumptions of the present refined plate theory are as follows:

(1) The displacements are small in comparison with the plate thickness and, therefore, strains involved are infinitesimal.

(2) The transverse displacement W includes two components of bending w_b and shear w_s. These components are functions of coordinates x, y only.

$$W(x,y,z) = w_b(x,y) + w_s(x,y) \tag{4}$$

(3) The transverse normal stress σ_z is negligible in comparison with in-plane stresses σ_x and σ_y.

(4) The displacements U in x-direction and V in y-direction consist of extension, bending and shear components.

$$\begin{cases} U = u + u_b + u_s \\ V = v + v_b + v_s \end{cases} \tag{5}$$

The bending components u_b and v_b are assumed to be similar to the displacements given by the classical plate theory. Therefore, the expressions for u_b and v_b can be given as

$$\begin{cases} u_b = -z\dfrac{\partial w_b}{\partial x} \\ v_b = -z\dfrac{\partial w_b}{\partial y} \end{cases} \tag{6a}$$

The shear components u_s and v_s, in conjunction with w_s, give rise to the parabolic variations of shear strains γ_{xz}, γ_{yz}, and hence to shear stresses τ_{xz}, τ_{yz} through the

thickness of the plate, in such a way that shear stresses τ_{xz}, τ_{yz} are zero at the top and bottom faces of the plate. Consequently, the expressions for u_s and v_s can be given as

$$\begin{cases} u_s = \left[\frac{1}{4}z - \frac{5}{3}z\left(\frac{z}{h}\right)^2\right]\frac{\partial w_s}{\partial x} \\ v_s = \left[\frac{1}{4}z - \frac{5}{3}z\left(\frac{z}{h}\right)^2\right]\frac{\partial w_s}{\partial y} \end{cases} \tag{6b}$$

2.4. Kinematics and constitutive equations

Based on the assumptions made in the preceding section, the displacement field can be obtained using Eqs. (4)-(6) as

$$\begin{cases} U(x,y,z) = u(x,y) - z\frac{\partial w_b}{\partial x} + z\left[\frac{1}{4} - \frac{5}{3}\left(\frac{z}{h}\right)^2\right]\frac{\partial w_s}{\partial x} \\ V(x,y,z) = v(x,y) - z\frac{\partial w_b}{\partial y} + z\left[\frac{1}{4} - \frac{5}{3}\left(\frac{z}{h}\right)^2\right]\frac{\partial w_s}{\partial y} \\ W(x,y,z) = w_b(x,y) + w_s(x,y) \end{cases} \tag{7}$$

The strains associated with the displacements in Eq. (7) are

$$\begin{cases} \varepsilon_x = \varepsilon_x^0 + z k_x^b + f k_x^s \\ \varepsilon_y = \varepsilon_y^0 + z k_y^b + f k_y^s \\ \gamma_{xy} = \gamma_{xy}^0 + z k_{xy}^b + f k_{xy}^s \\ \gamma_{yz} = g\,\gamma_{yz}^s \\ \gamma_{xz} = g\,\gamma_{xz}^s \\ \varepsilon_z = 0 \end{cases} \tag{8}$$

where

$$\begin{cases} \varepsilon_x^0 = \frac{\partial u}{\partial x}, \quad k_x^b = -\frac{\partial^2 w_b}{\partial x^2}, \quad k_x^s = -\frac{\partial^2 w_s}{\partial x^2} \\ \varepsilon_y^0 = \frac{\partial v}{\partial y}, \quad k_y^b = -\frac{\partial^2 w_b}{\partial y^2}, \quad k_y^s = -\frac{\partial^2 w_s}{\partial y^2} \\ \gamma_{xy}^0 = \frac{\partial u}{\partial y} + \frac{\partial v}{\partial x}, \quad k_{xy}^b = -2\frac{\partial^2 w_b}{\partial x \partial y} \\ k_{xy}^s = -2\frac{\partial^2 w_s}{\partial x \partial y} \\ \gamma_{yz}^s = \frac{\partial w_s}{\partial y}, \quad \gamma_{xz}^s = \frac{\partial w_s}{\partial x} \\ f = -\frac{1}{4}z + \frac{5}{3}z\left(\frac{z}{h}\right)^2, \quad g = \frac{5}{4} - 5\left(\frac{z}{h}\right)^2 \end{cases} \tag{9}$$

For elastic and isotropic FGMs, the constitutive relations can be written as

$$\begin{cases} \begin{bmatrix} \sigma_x \\ \sigma_y \\ \tau_{xy} \end{bmatrix} = \begin{bmatrix} Q_{11} & Q_{12} & 0 \\ Q_{12} & Q_{22} & 0 \\ 0 & 0 & Q_{66} \end{bmatrix} \begin{bmatrix} \varepsilon_x \\ \varepsilon_y \\ \gamma_{xy} \end{bmatrix} \\ \begin{bmatrix} \tau_{yz} \\ \tau_{zx} \end{bmatrix} = \begin{bmatrix} Q_{44} & 0 \\ 0 & Q_{55} \end{bmatrix} \begin{bmatrix} \gamma_{yz} \\ \gamma_{zx} \end{bmatrix} \end{cases} \tag{10}$$

where σ_x, σ_y τ_{xy}, τ_{yz} τ_{zx}, and ε_x, ε_y, γ_{xy}, γ_{yz}, γ_{zx} are the stress and strain components, respectively. Using the material properties defined in Eq. (3), stiffness coefficient Q_{ij} can be expressed as

$$\begin{cases} Q_{11} = Q_{22} = \frac{E(z)}{1-\nu^2} \\ Q_{12} = \frac{\nu E(z)}{1-\nu^2} \\ Q_{44} = Q_{55} = Q_{66} = \frac{E(z)}{2(1+\nu)} \end{cases} \tag{11}$$

2.5. Governing equations

The governing equations of equilibrium can be derived by using the principle of virtual displacements. The principle of virtual work in the present case yields

$$\int_{-h/2}^{h/2}\int_{\Omega}(\sigma_x\delta\varepsilon_x + \sigma_y\delta\varepsilon_y + \tau_{xy}\delta\gamma_{xy} + \tau_{yz}\delta\gamma_{yz} + \tau_{xz}\delta\gamma_{xz})\mathrm{d}\Omega\mathrm{d}z - \int_{\Omega} q\,\delta W\mathrm{d}\Omega = 0 \tag{12}$$

where Ω is the top surface, and q the external load.

Substituting Eqs. (7)-(8) and Eq. (10) into Eq. (12) and integrating through the thickness of the plate, Eq. (12) can be rewritten as

$$\int_{\Omega}(N_x\delta\varepsilon_x^0 + N_y\delta\varepsilon_y^0 + N_{xy}\delta\varepsilon_{xy}^0 + M_x^b\delta k_x^b + M_y^b\delta k_y^b + M_{xy}^b\delta k_{xy}^b + M_x^s\delta k_x^s + M_y^s\delta k_y^s + M_{xy}^s\delta k_{xy}^s + S_{yz}^s\delta\gamma_{yz}^s + S_{xz}^s\delta\gamma_{xz}^s)\mathrm{d}\Omega - \int_{\Omega} q(\delta w_b + \delta w_b)\,\mathrm{d}\Omega = 0 \tag{13}$$

where the stress resultants $\boldsymbol{N}$, $\boldsymbol{M}^b$, $\boldsymbol{M}^s$ and $\boldsymbol{S}$ are defined by

$$\begin{cases} [N_x \quad N_y \quad N_{xy}] = \int_{-h/2}^{h/2}[\sigma_x \quad \sigma_y \quad \tau_{xy}]\mathrm{d}z \\ [M_x^b \quad M_y^b \quad M_{xy}^b] = \int_{-h/2}^{h/2}[\sigma_x \quad \sigma_y \quad \tau_{xy}]z\mathrm{d}z \\ [M_x^s \quad M_y^s \quad M_{xy}^s] = \int_{-h/2}^{h/2}[\sigma_x \quad \sigma_y \quad \tau_{xy}]f\mathrm{d}z \\ [S_{xz}^s \quad S_{yz}^s] = \int_{-h/2}^{h/2}[\tau_{xz} \quad \tau_{yz}]g\mathrm{d}z \end{cases} \tag{14}$$

Substituting Eq. (10) into Eq. (14) and integrating through the thickness of the plate, the stress resultants are given as

$$\begin{cases} \begin{bmatrix} \boldsymbol{N} \\ \boldsymbol{M}^b \\ \boldsymbol{M}^s \end{bmatrix} = \begin{bmatrix} \boldsymbol{A} & \boldsymbol{B} & \boldsymbol{B}^s \\ \boldsymbol{B} & \boldsymbol{D} & \boldsymbol{D}^s \\ \boldsymbol{B}^s & \boldsymbol{D}^s & \boldsymbol{H}^s \end{bmatrix} \begin{bmatrix} \boldsymbol{\varepsilon} \\ \boldsymbol{k}^b \\ \boldsymbol{k}^s \end{bmatrix} \\ \begin{bmatrix} S_{yz}^s \\ S_{xz}^s \end{bmatrix} = \begin{bmatrix} A_{44}^s & 0 \\ 0 & A_{55}^s \end{bmatrix} \begin{bmatrix} \gamma_{yz}^s \\ \gamma_{xz}^s \end{bmatrix} \end{cases} \tag{15}$$

where

$$\begin{cases} \boldsymbol{N}=[N_x \quad N_y \quad N_{xy}]^{\mathrm{T}} \\ \boldsymbol{M}^{\mathrm{b}}=[M_x^{\mathrm{b}} \quad M_y^{\mathrm{b}} \quad M_{xy}^{\mathrm{b}}]^{\mathrm{T}} \\ \boldsymbol{M}^{\mathrm{s}}=[M_x^{\mathrm{s}} \quad M_y^{\mathrm{s}} \quad M_{xy}^{\mathrm{s}}]^{\mathrm{T}} \end{cases} \tag{16a}$$

$$\begin{cases} \boldsymbol{\varepsilon}=[\varepsilon_x^0 \quad \varepsilon_y^0 \quad \gamma_{xy}^0] \\ \boldsymbol{k}^{\mathrm{b}}=[k_x^{\mathrm{b}} \quad k_y^{\mathrm{b}} \quad k_{xy}^{\mathrm{b}}] \\ \boldsymbol{k}^{\mathrm{s}}=[k_x^{\mathrm{s}} \quad k_y^{\mathrm{s}} \quad k_{xy}^{\mathrm{s}}] \end{cases} \tag{16b}$$

$$\begin{cases} \boldsymbol{A}=\begin{bmatrix} A_{11} & A_{12} & 0 \\ A_{12} & A_{22} & 0 \\ 0 & 0 & A_{66} \end{bmatrix} \\ \boldsymbol{B}=\begin{bmatrix} B_{11} & B_{12} & 0 \\ B_{12} & B_{22} & 0 \\ 0 & 0 & B_{66} \end{bmatrix} \\ \boldsymbol{D}=\begin{bmatrix} D_{11} & D_{12} & 0 \\ D_{12} & D_{22} & 0 \\ 0 & 0 & D_{66} \end{bmatrix} \end{cases} \tag{16c}$$

$$\begin{cases} \boldsymbol{B}^{\mathrm{s}}=\begin{bmatrix} B_{11}^{\mathrm{s}} & B_{12}^{\mathrm{s}} & 0 \\ B_{12}^{\mathrm{s}} & B_{22}^{\mathrm{s}} & 0 \\ 0 & 0 & B_{66}^{\mathrm{s}} \end{bmatrix} \\ \boldsymbol{D}^{\mathrm{s}}=\begin{bmatrix} D_{11}^{\mathrm{s}} & D_{12}^{\mathrm{s}} & 0 \\ D_{12}^{\mathrm{s}} & D_{22}^{\mathrm{s}} & 0 \\ 0 & 0 & D_{66}^{\mathrm{s}} \end{bmatrix} \\ \boldsymbol{H}^{\mathrm{s}}=\begin{bmatrix} H_{11}^{\mathrm{s}} & H_{12}^{\mathrm{s}} & 0 \\ H_{12}^{\mathrm{s}} & H_{22}^{\mathrm{s}} & 0 \\ 0 & 0 & H_{66}^{\mathrm{s}} \end{bmatrix} \end{cases} \tag{16d}$$

where A_{ij}, B_{ij}, etc., are the plate stiffness, defined by

$$\begin{cases} [A_{ij} \quad B_{ij} \quad D_{ij} \quad E_{ij} \quad F_{ij} \quad H_{ij}]= \\ \quad \sum_{n=1}^{3}\int_{h_n}^{h_{n+1}}[1 \quad z \quad z^2 \quad z^3 \quad z^4 \quad z^6]\,Q_{ij}\mathrm{d}z \\ \quad (i,j=1,2,6) \\ B_{ij}^{\mathrm{s}}=-\dfrac{1}{4}B_{ij}+\dfrac{5}{3h^2}E_{ij} \qquad (i,j=1,2,6) \\ D_{ij}^{\mathrm{s}}=-\dfrac{1}{4}D_{ij}+\dfrac{5}{3h^2}F_{ij} \qquad (i,j=1,2,6) \\ H_{ij}^{\mathrm{s}}=\dfrac{1}{16}D_{ij}-\dfrac{5}{6h^2}F_{ij}+\dfrac{25}{9h^4}H_{ij} \qquad (i,j=1,2,6) \\ [A_{ij} \quad D_{ij} \quad F_{ij}]=\sum_{n=1}^{3}\int_{h_n}^{h_{n+1}}[1 \quad z^2 \quad z^4]\,Q_{ij}\mathrm{d}z \\ \quad (i,j=4,5) \\ A_{ij}^{\mathrm{s}}=\dfrac{25}{16}A_{ij}-\dfrac{25}{6h^2}D_{ij}+\dfrac{25}{h^4}F_{ij} \qquad (i,j=4,5) \end{cases} \tag{17}$$

The governing equations of equilibrium can be derived from Eq. (13) by integrating the displacement gradients by parts and setting the coefficients δu, δv, δw_{b}, and δw_{s} to zero separately. Thus, one can obtain the equilibrium equations associated with the present RPT for the FGM sandwich plate

$$\begin{cases} \delta u: \quad \dfrac{\partial N_x}{\partial x}+\dfrac{\partial N_{xy}}{\partial y}=0 \\ \delta v: \quad \dfrac{\partial N_{xy}}{\partial x}+\dfrac{\partial N_y}{\partial y}=0 \\ \delta w_{\mathrm{b}}: \quad \dfrac{\partial^2 M_x^b}{\partial x^2}+2\dfrac{\partial^2 M_{xy}^{\mathrm{b}}}{\partial x\partial y}+\dfrac{\partial^2 M_y^{\mathrm{b}}}{\partial y^2}+q=0 \\ \delta w_{\mathrm{s}}: \quad \dfrac{\partial^2 M_x^{\mathrm{s}}}{\partial x^2}+2\dfrac{\partial^2 M_{xy}^{\mathrm{s}}}{\partial x\partial y}+\dfrac{\partial^2 M_y^{\mathrm{s}}}{\partial y^2}+\dfrac{\partial S_{xz}^{\mathrm{s}}}{\partial x}+ \\ \qquad \dfrac{\partial S_{yz}^{\mathrm{s}}}{\partial y}+q=0 \end{cases} \tag{18}$$

Substituting Eq. (15) into Eq. (18), we obtain the following operator equation:

$$\boldsymbol{L}\boldsymbol{\delta}=\boldsymbol{f} \tag{19}$$

where $\boldsymbol{\delta}=[u \quad v \quad w_{\mathrm{b}} \quad w_{\mathrm{s}}]^{\mathrm{T}}$; $\boldsymbol{f}=[0 \quad 0 \quad q \quad q]^{\mathrm{T}}$ is a generalized force vector, and $\boldsymbol{L}$ is the symmetric matrix of differential operators,

$$\begin{cases} L_{11}=A_{11}d_{11}+A_{66}d_{22} \\ L_{12}=(A_{12}+A_{66})\,d_{12} \\ L_{13}=-B_{11}d_{111}-(B_{12}+2B_{66})d_{122} \\ L_{14}=-B_{11}^{\mathrm{s}}d_{111}-(B_{12}^{\mathrm{s}}+2B_{66}^{\mathrm{s}})d_{122} \\ L_{22}=A_{22}d_{22}+A_{66}d_{11} \\ L_{23}=-B_{22}d_{222}-(B_{12}+2B_{66})d_{112} \\ L_{24}=-B_{22}^{\mathrm{s}}d_{222}-(B_{12}^{\mathrm{s}}+2B_{66}^{\mathrm{s}})d_{112} \\ L_{33}=D_{11}d_{1111}+2(D_{12}+2D_{66})d_{1122}+ \\ \qquad D_{22}d_{2222} \\ L_{34}=D_{11}^{\mathrm{s}}d_{1111}+2(D_{12}^{\mathrm{s}}+2D_{66}^{\mathrm{s}})d_{1122}+ \\ \qquad D_{22}^{\mathrm{s}}d_{2222} \\ L_{44}=H_{11}^{\mathrm{s}}d_{1111}+2(H_{12}^{\mathrm{s}}+2H_{66}^{\mathrm{s}})d_{1122}+ \\ \qquad H_{22}^{\mathrm{s}}d_{2222}-A_{55}^{\mathrm{s}}d_{11}-A_{44}^{\mathrm{s}}d_{22} \end{cases} \tag{20}$$

in which d_{ij}, d_{ijl}, and d_{ijlm} are the following differential operators:

$$\begin{cases} d_{ij}=\dfrac{\partial^2}{\partial x_i\partial x_j}, \quad d_{ijl}=\dfrac{\partial^3}{\partial x_i\partial x_j\partial x_l} \\ d_{ijlm}=\dfrac{\partial^4}{\partial x_i\partial x_j\partial x_l\partial x_m} \qquad (i,j,l,m=1,2) \end{cases} \tag{21}$$

2.6. Analytical solutions for FGM sandwich plates

Rectangular FGM sandwich plates are generally classified in accordance with the type support used. We are here concerned with the analytical solutions of Eq. (19) for simply supported FGM sandwich plate. The following boundary conditions are imposed at the side edges.

$$\begin{cases} v(0,y)=w_{\mathrm{b}}(0,y)=w_{\mathrm{s}}(0,y)= \\ \qquad \dfrac{\partial w_{\mathrm{b}}}{\partial y}(0,y)=\dfrac{\partial w_{\mathrm{s}}}{\partial y}(0,y)=0 \\ v(a,y)=w_{\mathrm{b}}(a,y)=w_{\mathrm{s}}(a,y)= \\ \qquad \dfrac{\partial w_{\mathrm{b}}}{\partial y}(a,y)=\dfrac{\partial w_{\mathrm{s}}}{\partial y}(a,y)=0 \\ N_x(0,y)=M_x^{\mathrm{b}}(0,y)=M_x^{\mathrm{s}}(0,y)= \\ \qquad N_x(a,y)=M_x^{\mathrm{b}}(a,y)=M_x^{\mathrm{s}}(a,y)=0 \\ u(x,0)=w_{\mathrm{b}}(x,0)=w_{\mathrm{s}}(x,0)= \\ \qquad \dfrac{\partial w_{\mathrm{b}}}{\partial x}(x,0)=\dfrac{\partial w_{\mathrm{s}}}{\partial x}(x,0)=0 \\ u(x,b)=w_{\mathrm{b}}(x,b)=w_{\mathrm{s}}(x,b)= \\ \qquad \dfrac{\partial w_{\mathrm{b}}}{\partial x}(x,b)=\dfrac{\partial w_{\mathrm{s}}}{\partial x}(x,b)=0 \\ N_y(x,0)=M_y^{\mathrm{b}}(x,0)=M_y^{\mathrm{s}}(x,0)= \\ \qquad N_y(x,b)=M_y^{\mathrm{b}}(x,b)=M_y^{\mathrm{s}}(x,b)=0 \end{cases} \tag{22}$$

To solve this problem, Navier presented the external force for the case of sinusoidally distributed load as

$$q(x,y)=q_0\sin(\lambda x)\sin(\mu y)\,, \tag{23}$$

where $\lambda=\pi/a$ and $\mu=\pi/b$, and q_0 represents the intensity of the load at the plate center.

Following the Navier solution procedure, we assume the following solution form for $[u \quad v \quad w_{\mathrm{b}} \quad w_{\mathrm{s}}]$ that satisfies the boundary conditions,

$$\begin{bmatrix} u \\ v \\ w_{\mathrm{b}} \\ w_{\mathrm{s}} \end{bmatrix}=\begin{bmatrix} \overline{U}\cos(\lambda x)\sin(\mu y) \\ \overline{V}\sin(\lambda x)\cos(\mu y) \\ \overline{W}_{\mathrm{b}}\sin(\lambda x)\sin(\mu y) \\ \overline{W}_{\mathrm{s}}\sin(\lambda x)\sin(\mu y) \end{bmatrix} \tag{24}$$

where $\overline{U}$, $\overline{V}$, $\overline{W}_{\mathrm{b}}$ and $\overline{W}_{\mathrm{s}}$ are arbitrary parameters to be determined subject to the condition that the solution in Eq. (24) satisfies the basic Eq. (19). One obtains the following operator equation

$$\boldsymbol{K}\boldsymbol{\Delta}=\boldsymbol{F} \tag{25}$$

where $\boldsymbol{\Delta}$ and $\boldsymbol{F}$ denote the columns

$$\begin{cases} \boldsymbol{\Delta}=[\overline{U} \quad \overline{V} \quad \overline{W}_{\mathrm{b}} \quad \overline{W}_{\mathrm{s}}] \\ \boldsymbol{F}^{\mathrm{T}}=[0 \quad 0 \quad q_0 \quad q_0] \end{cases} \tag{26}$$

and

$$\boldsymbol{K}=\begin{bmatrix} a_{11} & a_{12} & a_{13} & a_{14} \\ a_{12} & a_{22} & a_{23} & a_{24} \\ a_{13} & a_{23} & a_{33} & a_{34} \\ a_{14} & a_{24} & a_{34} & a_{44} \end{bmatrix} \tag{27}$$

where

$$\begin{cases} a_{11}=A_{11}\lambda^2+A_{66}\mu^2 \\ a_{12}=\lambda\mu\,(A_{12}+A_{66}) \\ a_{13}=-\lambda\,[B_{11}\lambda^2+(B_{12}+2B_{66})\,\mu^2] \\ a_{14}=-\lambda\,[B_{11}^{\mathrm{s}}\lambda^2+(B_{12}^{\mathrm{s}}+2B_{66}^{\mathrm{s}})\,\mu^2] \\ a_{22}=A_{66}\lambda^2+A_{22}\mu^2 \\ a_{23}=-\mu\,[(B_{12}+2B_{66})\,\lambda^2+B_{22}\mu^2] \\ a_{24}=-\mu\,[(B_{12}^{\mathrm{s}}+2B_{66}^{\mathrm{s}})\,\lambda^2+B_{22}^{\mathrm{s}}\mu^2] \\ a_{33}=D_{11}\lambda^4+2(D_{12}+2D_{66})\lambda^2\mu^2+D_{22}\mu^4 \\ a_{34}=D_{11}^{\mathrm{s}}\lambda^4+2(D_{12}^{\mathrm{s}}+2D_{66}^{\mathrm{s}})\lambda^2\mu^2+D_{22}^{\mathrm{s}}\mu^4 \\ a_{44}=H_{11}^{\mathrm{s}}\lambda^4+2(H_{11}^{\mathrm{s}}+2H_{66}^{\mathrm{s}})\lambda^2\mu^2+ \\ \qquad H_{22}^{\mathrm{s}}\mu^4+A_{55}^{\mathrm{s}}\lambda^2+A_{44}^{\mathrm{s}}\mu^2 \end{cases} \tag{28}$$

3. Numerical Results and Discussion

In this study, static analysis of simply supported FGM plates by the present RPT is suggested for investigation. Navier solutions for bending analysis of FGM plates are presented by solving Eq. (25).

The static analysis is conducted for two combinations of metal and ceramic. The first set of materials chosen is aluminum and alumina. The second combination of materials consists of aluminum and zirconia. The material properties are as follow:

$$\begin{cases} \text{Ceramic (zirconia, } \mathrm{ZrO_2}\text{):} \\ \quad E_{\mathrm{c}}=151\ \text{GPa},\ \nu=0.3 \\ \text{Ceramic (alumina, } \mathrm{Al_2O_3}\text{):} \\ \quad E_{\mathrm{c}}=380\ \text{GPa},\ \nu=0.3 \\ \text{Metal (Aluminium, Al):} \\ \quad E_{\mathrm{m}}=70\ \text{GPa},\ \nu=0.3 \end{cases}$$

Numerical results are presented in terms of non-dimensional stresses and deflection. The various nondimensional parameters used are

$$\begin{cases} \text{Central deflection: } \overline{W}=\dfrac{10hE_0}{q_0a^2}W\left(\dfrac{a}{2},\dfrac{b}{2}\right) \\ \text{Axial stress: } \overline{\sigma}_x=\dfrac{10h^2}{q_0a^2}\sigma_x\left(\dfrac{a}{2},\dfrac{b}{2},\dfrac{h}{2}\right) \\ \text{Shear stress: } \overline{\tau}_{xz}=\dfrac{h}{q_0a}\tau_{xz}\left(0,\dfrac{b}{2},0\right) \end{cases}$$

where E_0=1 GPa. It is assumed (unless otherwise stated) that the plate is made from aluminium-zirconia FGM. We also take the shear correction factor K=5/6

in the first shear deformation plate theory (FSDPT).

In order to prove the validity of the present theory, results are obtained for fully FGM plates and compared with the existing ones in the literature [28-29]. For other verification, the results obtained for FGM sandwich plates using the present RPT are compared with other theories existing in the literature such as CPT, FSDPT, and higher-order shear deformation plate theories (HSDPT) such as: TSDPT and sinusoidal shear deformation plate theory (SSDPT) as shown in Table 1, in which ϕ_x and ϕ_y are the rotations of the normal of the midplane about y and x, respectively.

Table 2 presents the dimensionless deflections and stresses of the square FGM plate (a/h=10) for different values of the power-law k. It can be seen that the results obtained using the present RPT are identical to those of Zenkour [28].

Table 3 presents the central deflections and the transverse shear stresses of simply supported square FGM plate. The results are compared with those of 2D higher-order theory of Matsunaga [29]. It can be seen that the results agree well with that reported by Matsunaga [29].

Table 1 Kinematical assumptions of different plate theories

Theory	Assumption of three-dimensional displacements
CPT	$\begin{cases} U(x,y,z)=u(x,y)-z\dfrac{\partial w}{\partial x} \\ V(x,y,z)=v(x,y)-z\dfrac{\partial w}{\partial y} \\ W(x,y,z)=w(x,y) \end{cases}$
FSDPT	$\begin{cases} U(x,y,z)=u(x,y)+z\phi_x(x,y) \\ V(x,y,z)=v(x,y)+z\phi_y(x,y) \\ W(x,y,z)=w(x,y) \end{cases}$
TSDPT	$\begin{cases} U(x,y,z)=u(x,y)+z\phi_x(x,y)-\dfrac{4z^3}{3h^2}\left(\phi_x+\dfrac{\partial w}{\partial x}\right) \\ V(x,y,z)=v(x,y)+z\phi_y(x,y)-\dfrac{4z^3}{3h^2}\left(\phi_y+\dfrac{\partial w}{\partial y}\right) \\ W(x,y,z)=w(x,y) \end{cases}$
SSDPT	$\begin{cases} U(x,y,z)=u(x,y)-z\dfrac{\partial w}{\partial x}+\dfrac{h}{\pi}\sin\left(\dfrac{\pi z}{h}\right)\phi_x(x,y) \\ V(x,y,z)=v(x,y)-z\dfrac{\partial w}{\partial x}+\dfrac{h}{\pi}\sin\left(\dfrac{\pi z}{h}\right)\phi_y(x,y) \\ W(x,y,z)=w(x,y) \end{cases}$

Table 2 Comparison of dimensionless deflections and stresses in square FGM plates (Al/Al_2O_3) subject to sinusoidal distributed load

k	$\overline{W}=\dfrac{10h^3E_c}{a^4q_0}W\left(\dfrac{a}{2},\dfrac{b}{2}\right)$		$\overline{\sigma}_x=\dfrac{h}{aq_0}\sigma_x\left(\dfrac{a}{2},\dfrac{b}{2},\dfrac{h}{2}\right)$		$\overline{\tau}_{xz}=\dfrac{h}{aq_0}\tau_{xz}\left(0,\dfrac{b}{2},0\right)$	
	Ref. [28]	Present RPT	Ref. [28]	Present RPT	Ref. [28]	Present RPT
Ceramic	0.296 0	0.296 1	1.995 5	1.994 3	0.246 2	0.238 6
1	0.588 9	0.589 0	3.087 0	3.085 0	0.246 2	0.238 6
2	0.757 3	0.757 3	3.609 4	3.606 7	0.226 5	0.218 6
3	0.837 7	0.837 5	3.874 2	3.870 9	0.210 7	0.202 4
4	0.881 9	0.881 6	4.069 3	4.065 5	0.202 9	0.194 4
5	0.911 8	0.911 2	4.248 8	4.244 7	0.201 7	0.193 0
6	0.935 6	0.935 2	4.424 4	4.420 1	0.204 1	0.195 4
7	0.956 2	0.955 7	4.597 1	4.592 8	0.208 1	0.199 4
8	0.975 0	0.974 3	4.766 1	4.761 9	0.212 4	0.203 7
9	0.992 5	0.992 2	4.930 3	4.926 1	0.216 4	0.207 8
10	1.008 9	1.008 5	5.089 0	5.084 9	0.219 8	0.211 4
Metal	1.607 0	1.607 4	1.995 5	1.994 3	0.246 2	0.238 6

Table 3 Comparison of dimensionless deflections and transverse shear stresses in square FGM plates (Al/Al_2O_3) subject to sinusoidal distributed load.

a/h	k	$\overline{W}=WE_c/(q_0h)$		$\overline{\tau}_{xz}=\tau_{xz}(0,b/2)/q_0$	
		Ref. [29]	Present RPT	Ref. [29]	Present RPT
5	0	0.209 8	0.214 6	0.118 6	0.119 0
	0.5	0.317 9	0.323 5	0.120 9	0.121 7
	1.0	0.413 9	0.418 0	0.118 4	0.119 0
	4.0	0.651 1	0.650 6	0.107 6	0.096 9
	10.0	0.762 4	0.767 2	0.107 8	0.105 3
10	0	0.294 3	0.296 1	0.238 3	0.238 5
	0.5	0.450 4	0.453 7	0.243 1	0.243 9
	1.0	0.587 5	0.589 0	0.238 3	0.238 5
	4.0	0.882 3	0.881 6	0.217 5	0.194 3
	10.0	0.100 7	1.008 5	0.216 7	0.211 3

The numerical results of simply supported square FGM plates of Type A are presented in Tables 4-6. These tables consider the case of homogeneous hard-core in which the elastic modulus of Layer 1 are E_c=151 Gpa (P_1, zirconia) at the top face and E_m= 70 Gpa (P_2, aluminium) at the bottom face. The results are considered for k = 0, 1, 2, 5, 10 and different types of sandwich plates. It can be seen that the results obtained by TSDPT and the present RPT are identical. Table 4 shows that the effect of shear deformation is to increase the deflection. The difference between the shear deformation theories is insignificant for fully ceramic plates (k = 0). It is to be noted that the CPT yields identical axial stresses with the FSDPT and so Table 5 lacks the results of CPT. The difference between several kinds of sandwich plates is insignificant for fully ceramic plates (k = 0). The axial stress is very sensitive to the variation of k. Table 6 shows that the transverse shear stresses as per the FSDPT may be indistinguishable. The difference between several kinds of sandwich plates is insignificant for fully ceramic plates (k = 0). The values of the transverse shear stresses decrease as k decreases for the FGM plates with homogeneous hardcore.

Table 4 Comparisons of dimensionless deflection of simply supported square power-law FGM plates with other theories (*a/h*=10)

k	Theory	$\overline{W}$				
		1-0-1	2-1-2	1-1-1	2-2-1	1-2-1
0	Present RPT	0.196 06	0.196 06	0.196 06	0.196 06	0.196 06
	SSDPT	0.196 05	0.196 05	0.196 05	0.196 05	0.196 05
	TSDPT	0.196 06	0.196 06	0.196 06	0.196 06	0.196 06
	FSDPT	0.196 07	0.196 07	0.196 07	0.196 07	0.196 07
	CPT	0.185 60	0.185 60	0.185 60	0.185 60	0.185 60
1	Present RPT	0.323 58	0.306 31	0.291 99	0.280 85	0.270 94
	SSDPT	0.323 49	0.306 24	0.291 94	0.280 82	0.270 93
	TSDPT	0.323 58	0.306 32	0.291 99	0.280 85	0.270 94
	FSDPT	0.324 84	0.307 50	0.293 01	0.281 68	0.271 67
	CPT	0.310 54	0.294 17	0.280 26	0.269 20	0.259 58
2	Present RPT	0.373 34	0.352 31	0.332 88	0.316 16	0.302 63
	SSDPT	0.373 19	0.352 18	0.332 80	0.316 11	0.302 60
	TSDPT	0.373 35	0.352 31	0.332 89	0.316 17	0.302 63
	FSDPT	0.375 14	0.354 08	0.334 41	0.317 38	0.303 70
	CPT	0.358 85	0.339 42	0.320 67	0.304 05	0.290 95
5	Present RPT	0.409 27	0.391 82	0.371 44	0.349 60	0.334 80
	SSDPT	0.409 05	0.391 60	0.371 28	0.349 50	0.334 74
	TSDPT	0.409 27	0.391 83	0.371 45	0.349 60	0.334 80
	FSDPT	0.411 20	0.394 18	0.373 56	0.351 23	0.336 31
	CPT	0.392 27	0.377 89	0.358 65	0.336 93	0.322 83
10	Present RPT	0.417 72	0.404 07	0.385 51	0.362 12	0.348 23
	SSDPT	0.417 50	0.403 76	0.384 90	0.349 16	0.341 19
	TSDPT	0.417 72	0.404 07	0.385 51	0.362 15	0.348 24
	FSDPT	0.419 19	0.406 57	0.387 87	0.363 95	0.349 96
	CPT	0.398 76	0.389 41	0.372 36	0.349 15	0.336 12

Table 5 Comparisons of dimensionless axial stress of simply supported square power-law FGM plates with other theories (*a/h*=5)

k	Theory	$\overline{\sigma}_x$				
		1-0-1	2-1-2	1-1-1	2-2-1	1-2-1
0	Present RPT	2.049 85	2.049 85	2.049 85	2.049 85	2.049 85
	SSDPT	2.054 52	2.054 52	2.054 52	2.054 52	2.054 52
	TSDPT	2.049 85	2.049 85	2.049 85	2.049 85	2.049 85
	FSDPT	1.975 76	1.975 76	1.975 76	1.975 76	1.975 76
1	Present RPT	1.579 23	1.495 87	1.426 17	1.320 62	1.323 09
	SSDPT	1.582 04	1.498 59	1.428 92	1.323 42	1.325 90
	TSDPT	1.579 23	1.495 87	1.426 17	1.320 62	1.323 09
	FSDPT	1.532 45	1.451 67	1.383 03	1.277 49	1.280 96
2	Present RPT	1.821 67	1.721 44	1.627 48	1.470 95	1.479 88
	SSDPT	1.824 50	1.724 12	1.630 25	1.473 87	1.482 83
	TSDPT	1.821 67	1.721 44	1.627 48	1.470 95	1.479 88
	FSDPT	1.770 85	1.674 96	1.582 42	1.425 28	1.435 80
5	Present RPT	1.992 72	1.913 02	1.815 80	1.611 81	1.638 14
	SSDPT	1.995 67	1.915 47	1.818 38	1.614 77	1.641 06
	TSDPT	1.992 72	1.913 02	1.815 80	1.611 81	1.638 14
	FSDPT	1.935 76	1.864 79	1.769 88	1.564 01	1.593 09
10	Present RPT	2.030 36	1.971 26	1.883 77	1.664 80	1.703 83
	SSDPT	2.033 60	1.973 13	1.881 47	1.619 79	1.648 51
	TSDPT	2.030 36	1.971 26	1.883 76	1.666 60	1.704 17
	FSDPT	1.967 80	1.921 65	1.837 54	1.616 45	1.658 44

In general, the fully ceramic plates give the smallest deflections and shear stresses and the largest axial stresses. As the volume fraction exponent increases for FGM plates, the deflection, axial stress and shear stress will increase. These results will decrease as the core thickness, with respect to the total thickness of the plate, increases. In fact the non-symmetric 2-2-1 FGM plate yields the smallest axial stresses.

The comparisons of the maximum deflections are given in Table 7 for FGM sandwich plate with homogeneous hardcore and with volume fraction indices $k = 2$. It can be observed that the results obtained by the present RPT are identical to those of TSDPT. In addition, the deflection will decrease as the aspect ratio a/b increases.

Table 6 Comparisons of dimensionless transverse shear stress of simply supported square power-law FGM plates with other theories (*a/h*=5)

k	Theory	$\overline{\tau}_{xz}$				
		1-0-1	2-1-2	1-1-1	2-2-1	1-2-1
0	Present RPT	0.238 57	0.238 57	0.238 57	0.238 57	0.238 57
	SSDPT	0.246 18	0.246 18	0.246 18	0.246 18	0.246 18
	TSDPT	0.238 57	0.238 57	0.238 57	0.238 57	0.238 57
	FSDPT	0.190 99	0.190 99	0.190 99	0.190 99	0.190 99
1	Present RPT	0.292 02	0.271 04	0.261 16	0.259 50	0.252 58
	SSDPT	0.299 07	0.277 74	0.268 09	0.266 80	0.260 04
	TSDPT	0.292 03	0.271 04	0.261 17	0.259 51	0.252 58
	FSDPT	0.260 99	0.243 16	0.232 57	0.227 62	0.220 57
2	Present RPT	0.326 22	0.288 38	0.271 87	0.269 39	0.258 33
	SSDPT	0.332 85	0.294 22	0.278 07	0.276 27	0.265 43
	TSDPT	0.326 22	0.288 38	0.271 88	0.269 39	0.258 34
	FSDPT	0.297 31	0.267 52	0.250 77	0.243 16	0.232 57
5	Present RPT	0.386 34	0.314 54	0.286 42	0.282 65	0.265 12
	SSDPT	0.393 70	0.319 30	0.291 50	0.288 95	0.271 53
	TSDPT	0.386 34	0.314 54	0.286 43	0.282 65	0.265 12
	FSDPT	0.345 38	0.297 31	0.272 06	0.260 99	0.245 96
10	Present RPT	0.432 06	0.332 42	0.295 66	0.290 83	0.268 94
	SSDPT	0.441 47	0.336 44	0.295 29	0.296 71	0.276 76
	TSDPT	0.432 06	0.332 42	0.295 66	0.290 80	0.268 95
	FSDPT	0.372 77	0.313 16	0.282 99	0.269 98	0.252 57

Table 7 Effect of aspect ratio *a*/*b* on the dimensionless deflection of FGM sandwich plates (*a/h*=10 and *k*=2).

Scheme	Theory	$\overline{W}$				
		a/*b*=1/3	*a*/*b*=0.5	*a*/*b*=1	*a*/*b*=1.5	*a*/*b*=2
1-0-1	Present RPT	1.188 77	0.941 85	0.373 35	0.144 81	0.063 21
	SSDPT	1.188 49	0.941 60	0.373 19	0.144 72	0.063 15
	TSDPT	1.188 77	0.941 86	0.373 35	0.144 81	0.063 21
	FSDPT	1.192 00	0.944 73	0.375 14	0.145 92	0.063 93
	CPT	1.162 67	0.918 65	0.358 85	0.135 90	0.057 42
2-1-2	Present RPT	1.122 93	0.889 54	0.352 31	0.136 47	0.059 46
	SSDPT	1.122 69	0.889 33	0.352 18	0.136 39	0.059 41
	TSDPT	1.122 93	0.889 55	0.352 31	0.136 47	0.059 46
	FSDPT	1.126 11	0.892 37	0.354 08	0.137 56	0.060 17
	CPT	1.099 71	0.868 91	0.339 42	0.128 54	0.054 31
1-1-1	Present RPT	1.060 96	0.840 46	0.332 88	0.128 95	0.056 19
	SSDPT	1.060 80	0.840 32	0.332 80	0.128 90	0.056 15
	TSDPT	1.060 96	0.840 46	0.332 89	0.128 95	0.056 19
	FSDPT	1.063 69	0.842 89	0.334 41	0.129 89	0.056 80
	CPT	1.038 95	0.820 90	0.320 67	0.121 44	0.051 31
2-2-1	Present RPT	1.006 94	0.797 76	0.316 17	0.122 60	0.053 49
	SSDPT	1.006 83	0.797 67	0.316 11	0.122 56	0.053 47
	TSDPT	1.006 94	0.797 76	0.316 17	0.122 60	0.053 49
	FSDPT	1.009 11	0.799 69	0.317 38	0.123 34	0.053 98
	CPT	0.985 12	0.778 37	0.304 05	0.115 14	0.048 65
1-2-1	Present RPT	0.963 71	0.763 53	0.302 63	0.117 37	0.051 22
	SSDPT	0.963 66	0.763 48	0.302 60	0.117 35	0.051 21
	TSDPT	0.963 71	0.763 53	0.302 63	0.117 37	0.051 22
	FSDPT	0.965 63	0.765 24	0.303 70	0.108 03	0.051 65
	CPT	0.942 69	0.744 84	0.290 95	0.110 18	0.046 55

The central deflections due to flexure $\bar{w}_b$ and shear $\bar{w}_s$ are calculated, and then are summed up to get the total deflections $\bar{W}$. These results are shown in Table 8 for square power-law FGM plates of Type A with homogeneous softcore in which the elastic modulus of Layer 1 is E_m=70 GPa (P_1, aluminum) at the top face and E_c=151 GPa (P_2, zirconia) at the bottom face. The error level increases with the decrease in the thickness ratio a/h. Hence, the shear effect is more pronounced for smaller thickness ratio a/h. The results emphasize also the great influence exerted by the volume fraction indices k on the analyzed deflections.

Table 8 Dimensionless deflection of square FGM sandwich plates with shear effect

a/h	k	2-1-2			
		$\bar{w}_s$	$\bar{w}_b$	$\bar{W}$	Error/%
2	0	0.022 20	0.016 01	0.038 21	58.10
	2	0.016 32	0.007 90	0.024 22	67.38
	5	0.014 62	0.007 55	0.022 17	65.94
5	0	0.022 51	0.100 09	0.122 61	18.36
	2	0.016 63	0.050 42	0.067 05	24.80
	5	0.014 88	0.047 64	0.062 52	23.80
10	0	0.022 56	0.400 37	0.422 93	5.33
	2	0.020 22	0.166 75	0.186 97	10.81
	5	0.014 93	0.190 78	0.205 71	7.26
100	0	0.022 58	40.037 33	40.059 91	0.056 4
	2	0.016 69	20.245 68	20.262 37	0.082 4
	5	0.014 94	19.086 83	19.101 77	0.078 2

Figs. 3-8 present some numerical results of simply supported square power-law FGM plates of Type A using the present RPT. Figs. 3-5 consider the case of homogeneous hardcore in which the elastic modulus of Layer 1 is E_c=151 GPa (P_1, zirconia) at the top face and E_m=70 GPa (P_2, aluminum) at the bottom face. Figs. 6-8 consider the case of homogeneous softcore in which the elastic modulus of Layer 1 is E_m=70 GPa (P_1, aluminum) at the top face and E_c=151 GPa (P_2, zirconia) at the bottom face.

Fig.3 shows the variation of the center deflection

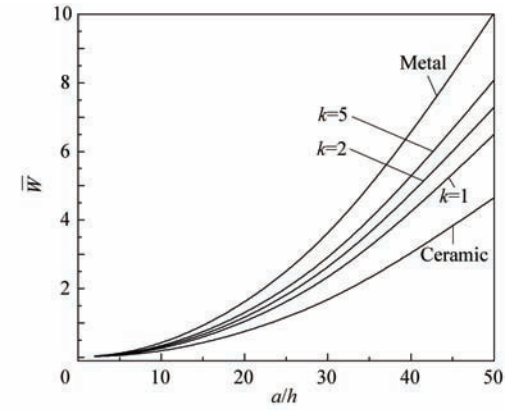

(a) The 1-2-1 FGM sandwich plate

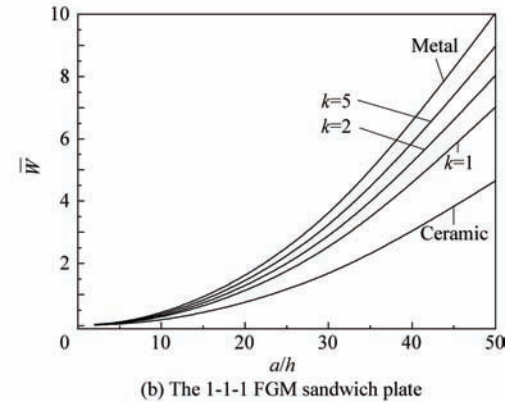

(b) The 1-1-1 FGM sandwich plate

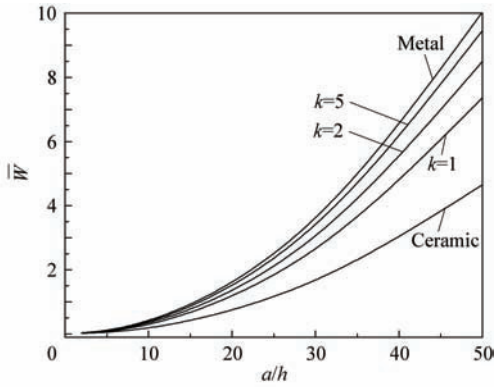

(c) The 2-1-2 FGM sandwich plate

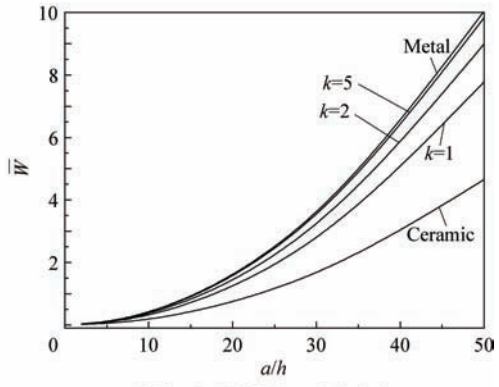

(d) The 1-0-1 FGM sandwich plate

Fig. 3 Dimensionless center deflection $\bar{W}$ as a function of side-to-thickness ratio a/h of FGM sandwich plate (Type A) with homogeneous hardcore for various values of k and different types of sandwich plates.

with side-to-thickness ratio a/h for different types of FGM symmetric plates with a homogeneous hardcore. The deflection of the metallic plate is found to be the largest magnitude and that of the ceramic plate of the smallest magnitude. The deflections of the FGM sandwich plates increase when $a/h \geq 5$. All the plates

with intermediate properties undergo corresponding intermediate values of center deflection. This is expected because the metallic plate is the one with the lowest stiffness and the ceramic plate is the one with the highest stiffness.

Fig. 4 contains the plots of the axial stress $\bar{\sigma}_x$ through the thickness of the plate with a homogeneous hardcore and for $k = 0$, 1, 2. Under the application of the sinusoidal loading, the stresses are tensile at the top surface and compressive at the bottom surface. The homogeneous ceramic plate ($k = 0$) yields the maximum compressive (tensile) stress at the bottom (top) surface. These are the metal-rich surfaces for the FGM plates ($k = 1$, 2). Note that for the different volume fraction exponents chosen, the plate corresponding to $k = 2$ yields the maximum compressive (tensile) stress at the bottom (top) surface of the core layer (see Figs. 4(a)-4(c). These are the ceramic-rich surfaces in which the ceramic plates experience the minimum compressive or tensile stresses. The stress profile for plate made of pure material (ceramic) changes linearly through the thickness. However, the axial stress variation is not linear for FGM plate.

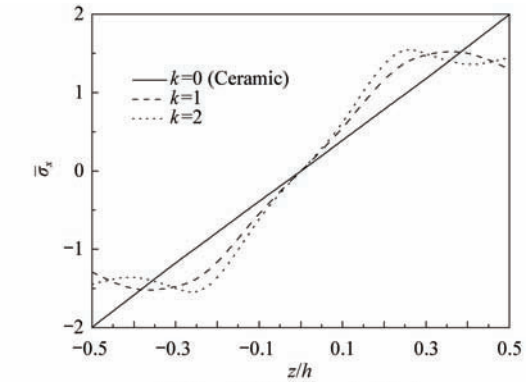

(a) The 1-2-1 FGM sandwich plate

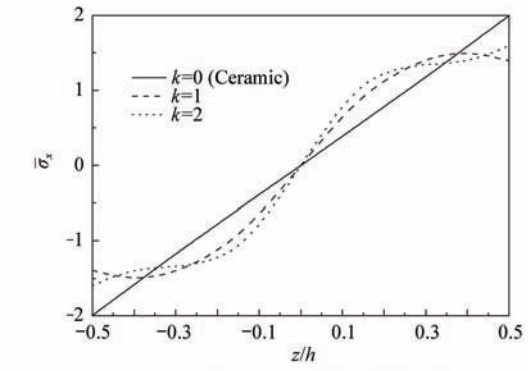

(b) The 1-1-1 FGM sandwich plate

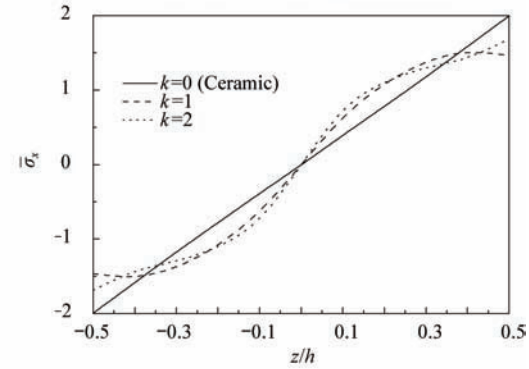

(c) The 2-1-2 FGM sandwich plate

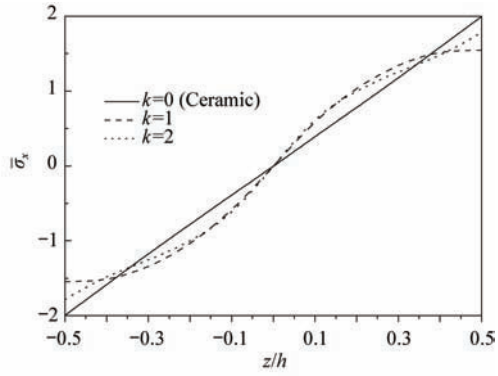

(d) The 1-0-1 FGM sandwich plate

Fig. 4 Variation of normal stress $\bar{\sigma}_x$ through plate thickness of FGM sandwich plate (Type A) with homogeneous hardcore for various values of k and different types of sandwich plates (a/h=10).

In Fig. 5 we have plotted the transverse shear stress $\bar{\tau}_{xz}$ through the thickness of the plate with a homogeneous hardcore and for $k = 0$, 1, 2. The maximum value occurs at a point on the mid-plane of the plate and its magnitude for FGM plate is larger than that for homogeneous ceramic plate ($k = 0$).

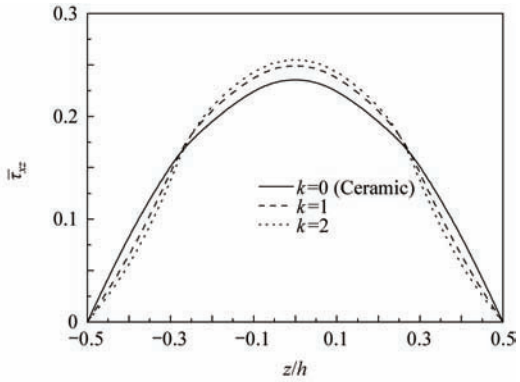

(a) The 1-2-1 FGM sandwich plate

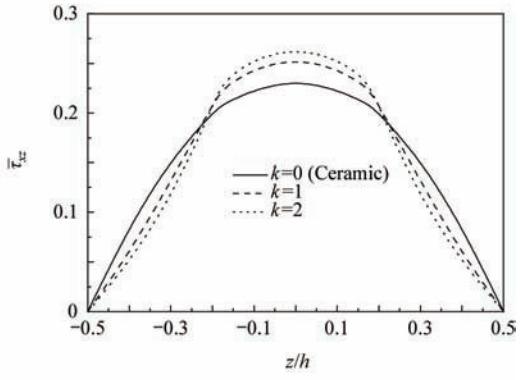

(b) The 1-1-1 FGM sandwich plate

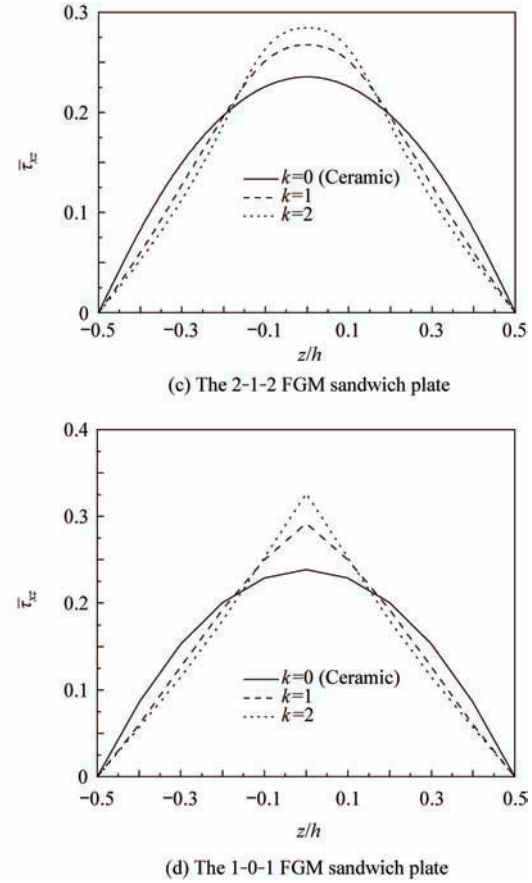

Fig. 5 Variation of transverse shear stress $\bar{\tau}_{xz}$ through plate thickness of FGM sandwich plate (Type A) with homogeneous hardcore for various values of k and different types of sandwich plates (a/h=10).

Fig. 6 shows the variation of the center deflection with side-to-thickness ratio for different types of FGM symmetric plates with a homogeneous softcore in which the elastic modulus of Layer 1 is E_m=70 GPa (P_1, aluminum) at the top surface and E_c=151 GPa (P_2, zirconia) at the bottom surface. Contrary to the case of homogeneous hardcore, it can be observed that for FGM plates with a homogeneous softcore, transverse deflection decreases as power law exponent k is increased. All the plates with intermediate properties undergo corresponding intermediate values of center deflection. This is expected because the metallic plate is the one with the lowest stiffness and the ceramic plate is the one with the highest stiffness.

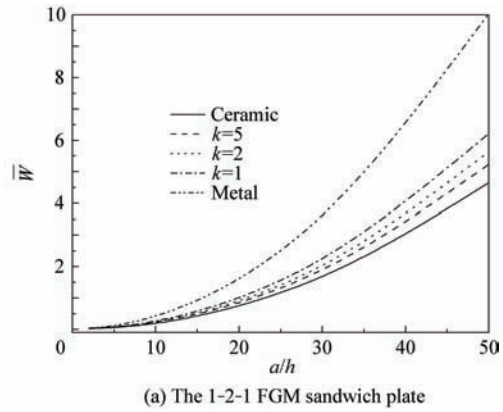

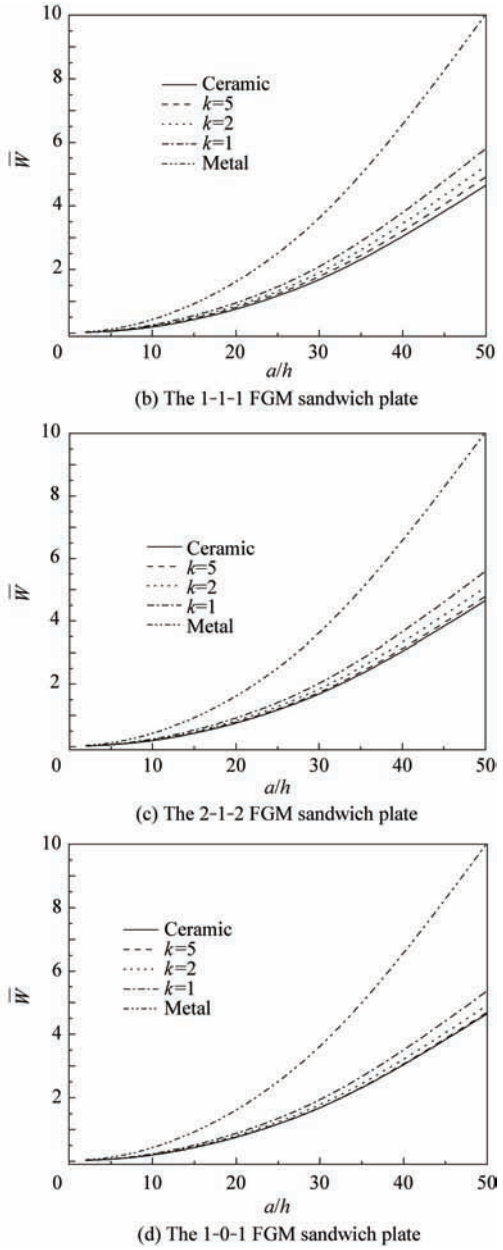

Fig. 6 Dimensionless center deflection $\bar{W}$ as a function of side-to-thickness ratio a/h of FGM sandwich plate (Type A) with homogeneous softcore for various values of k and different types of sandwich plates.

Fig. 7 depicts the through-the-thickness distributions of the axial stress $\bar{\sigma}_x$ in the FGM sandwich plate with a homogeneous softcore and for k = 0, 1, 2. The stresses are tensile at the top surface and compressive at the bottom surface. The homogeneous metal plate (k = 0) yields the maximum compressive (tensile) stress at the bottom (top) surface. The stress profile for plate made of pure material (metal) changes linearly through the thickness. However, the axial stress variation is not linear for FGM plate.

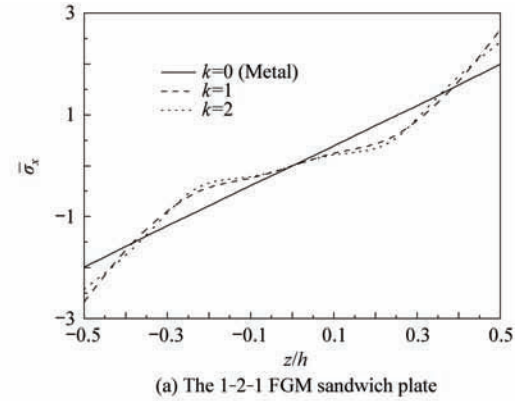

(a) The 1-2-1 FGM sandwich plate

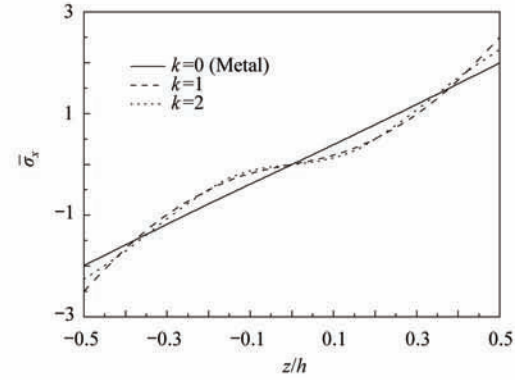

(b) The 1-1-1 FGM sandwich plate

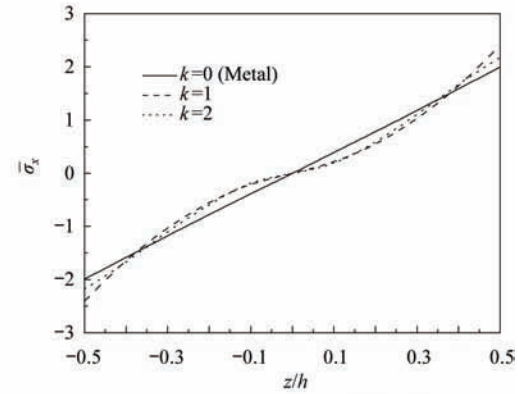

(c) The 2-1-2 FGM sandwich plate

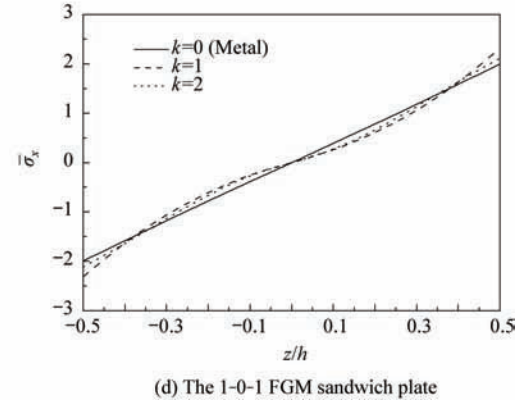

(d) The 1-0-1 FGM sandwich plate

Fig. 7 Variation of normal stress $\bar{\sigma}_x$ through plate thickness of FGM sandwich plate (Type A) with homogeneous softcore for various values of k and different types of sandwich plates (a/h=10).

The plot of shear stress $\bar{\tau}_{xz}$ across the FGM sandwich plate with a homogeneous softcore is presented in Fig. 8. The maximum value occurs at a point on the mid-plane of the plate and its magnitude for homogeneous metal plate ($k = 0$) is larger than that for FGM plate.

Using the present RPT, we present in Figs. 9-11 the center deflection $\overline{W}$, axial stress $\bar{\sigma}_x$ and transverse shear stress $\bar{\tau}_{xz}$ for the 1-4-1 sandwich plate of Type B (FGM core) with $k = 1, 2, 5$. P_1 is referred to the properties of aluminum and P_2 the properties of zirconia. In this case, the FGM core is metal-rich at the top surface and ceramic-rich at the bottom surface.

Fig. 9 shows the variation of the center deflection for various power law exponent k and with the side-to-thickness ratios. The FGM plate deflection is between those of plate made of ceramic and metal.

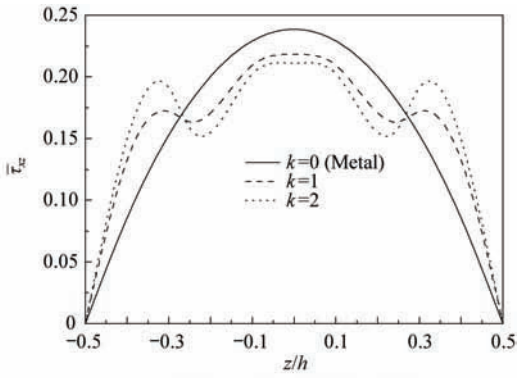

(a) The 1-2-1 FGM sandwich plate

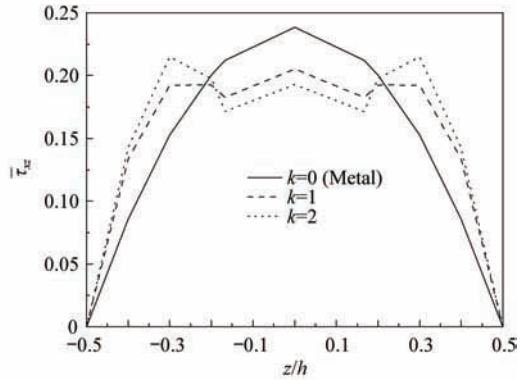

(b) The 1-1-1 FGM sandwich plate

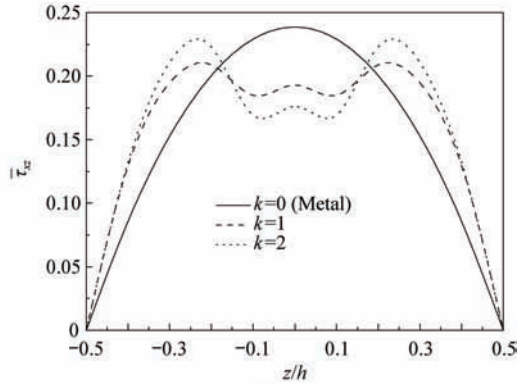

(c) The 2-1-2 FGM sandwich plate

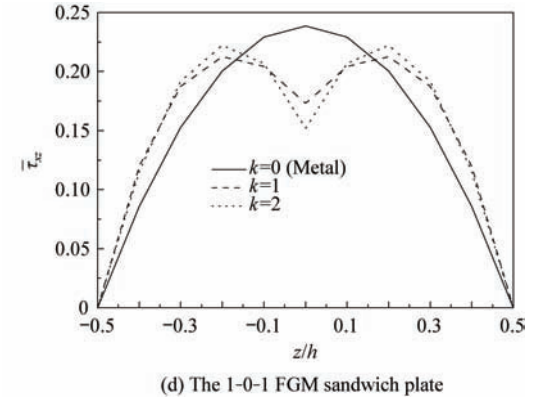

Fig. 8 Variation of transverse shear stress $\bar{\tau}_{xz}$ through plate thickness of FGM sandwich plate (Type A) with homogeneous softcore for various values of k and different types of sandwich plates (a/h=10).

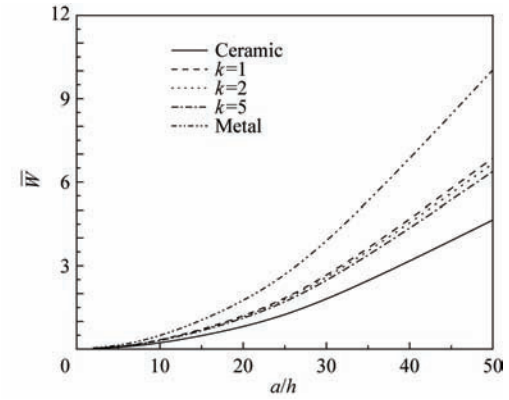

Fig. 9 Dimensionless center deflection $\overline{W}$ of the 1-4-1 sandwich square plate with FGM core.

As exhibited in Fig. 10, the axial stress, $\bar{\sigma}_x$, is compressive throughout the plate up to almost $\bar{z}$ = z/h= –0.06 and then they become tensile. The maximum compressive stresses occur at a point on the bottom surface and the maximum tensile stresses occur, of course, at a point on the top surface of the FGM plate.

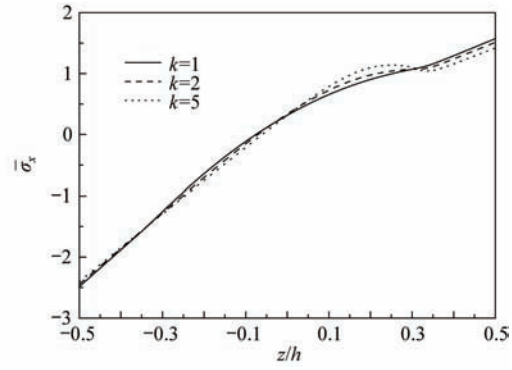

Fig. 10 Dimensionless axial stresses $\bar{\sigma}_x$ of the 1-4-1 sandwich square plate with FGM core (a/h=10).

Fig. 11 depicts the through-the-thickness distributions of the shear stresses $\bar{\tau}_{xz}$ in the square FGM sandwich plate. Contrary to the plate of Type A, the distribution of the shear stress is not symmetric in the case of sandwich plate of Type B (FGM core).

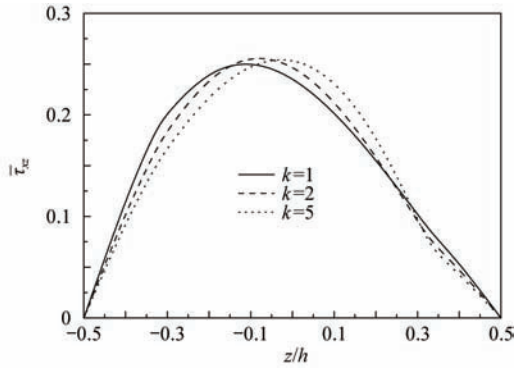

Fig. 11 Dimensionless transverse shear stresses $\bar{\tau}_{xz}$ of the 1-4-1 sandwich square plate with FGM core (a/h= 10).

4. Conclusions

A two variable refined theory is extended to the bending response of rectangular FGM sandwich plates. The number of primary variables in this theory is even less than that of first- and higher-order shear deformation plate theories. Hence, unlike any other theory, the theory presented gives rise to only four governing equations resulting in considerably lower computational effort when compared with the other higher-order theories reported in the literature having more numbers of governing equations. The theory accounts for parabolic distribution of the transverse shear strains through the plate thickness, and satisfies the zero traction boundary conditions on the surfaces of the plate without using shear correction factors. The accuracy and efficiency of the present theory have been demonstrated for bending behavior of simply supported FGM sandwich plates. The power-law FGM sandwich plates with FGM facesheet and homogeneous core, and the sandwich plates with homogeneous facesheet and FGM core are considered. The center deflection, axial stress and transverse shear stress predicted by the present theory (with four unknowns) and TSDPT (five unknowns) are identical.

In conclusion, it can be said that the proposed theory is not only accurate but also efficient in predicting the deflection and stresses of FGM sandwich plates.

References

[1] Yamanouchi M, Koizumi M, Shiota I. Functionally gradient materials. Proceedings of the First International Symposium on Functionally Gradient Materials. 1990.

[2] Fukui Y. Fundamental investigation of functionally gradient material manufacturing system using centrifugal force. Japan Society Mechanical Engineers International Journal 1991; 34(1): 144-148.

[3] Koizumi M. FGM activities in Japan. Composites Part

B: Engineering 1997; 28(1-2): 1-4.
[4] Fukui Y, Yamanaka N, Enokida Y. Bending strength of an Al-Al_3Ni functionally graded material. Composites Part B: Engineering 1997; 28(1-2): 37-43.
[5] Lambros J, Santare M H, Li H, et al. A novel technique for the fabrication of laboratory scale model of FGM. Experimental Mechanics 1999; 39(3): 184-190.
[6] Sarkar P, Datta S, Nicholson P S. Functionally graded ceramic/ceramic and metal/ceramic composites by electrophoretic deposition. Composites Part B: Engineering 1997; 28(1-2): 49-56.
[7] El-Hadek M, Tippur H V. Dynamic fracture parameters and constraint effects in functionally graded syntactic epoxy foams. International Journal of Solids Structures 2003; 40(8): 1885-1906.
[8] Reissner E. The effects of transverse shear deformation on the bending of elastic plates. ASME Journal of Applied Mechanics 1945; 12(2): 69-77.
[9] Midlin R D. Influence of rotary inertia and shear on flexural motion of isotropic elastic plates. ASME Journal of Applied Mechanics 1951; 18(2): 31-38.
[10] Yang P C, Norris C H, Stavsky Y. Elastic wave propagation in heterogeneous plates. International Journal of Solids and Structures 1966; 2(4): 665-684.
[11] Whitney J M, Pagano N J. Shear deformation in heterogeneous anisotropic plates. Journal of Applied Mechanics 1970; 37(4): 1031-1036.
[12] Essenburg F. On the significance of the inclusion of the effect of transverse normal strain in problems involving beams with surface constraints. ASME Journal of Applied Mechanics 1975; 42(1): 127-132.
[13] Reissner E. On transverse bending of plates, including the effects of transverse shear deformation. International Journal of Solids and Structures 1975; 11(5): 569-573.
[14] Lo K H, Christensen R M, Wu E M. A higher-order theory of plate deformation, Part 1: homogeneous plates. ASME Journal of Applied Mechanics 1977; 44(4): 663-668.
[15] Lo K H, Christensen R M, Wu E M. A higher-order theory of plate deformation, Part 2: laminate plates. ASME Journal of Applied Mechanics 1977; 44(4): 669-676.
[16] Reddy J N. A simple higher-order theory for laminated composite plates. Journal for Applied Mechanics 1984; 51(4): 745-752.
[17] Venkataraman S, Sankar B V. Analysis of sandwich beams with functionally graded core. AIAA-2001-1281, 2001.
[18] Anderson T A. A 3-D elasticity solution for a sandwich composite with functionally graded core subjected to transverse loading by a rigid sphere. Composite Structures 2003; 60(3): 265-274.
[19] Pan E, Han F. Exact solution for functionally graded and layered magneto-electro-elastic plates. International Journal of Engineering Science 2005; 43(3-4): 321-339.
[20] Das M, Barut A, Madenci E, et al. A triangular plate element for thermo-elastic analysis of sandwich panels with a functionally graded core. International Journal for Numerical Method in Engineering 2006; 68(9): 940-966.
[21] Shen H S. Postbuckling of FGM plates with piezoelectric actuators under thermo-electro-mechanical loadings. International Journal of Solids and Structures 2005; 42(23): 6101-6121.
[22] Noda N. Thermal stress in functionally graded materials. Third International Congress on Thermal Stresses, Thermal Stresses' 99. 1999.
[23] Shimpi R P. Refined plate theory and its variants. AIAA Journal 2002; 40(1): 137-146.
[24] Shimpi R P, Patel H G. A two variable refined plate theory for orthotropic plate analysis. International Journal of Solids Structure 2006; 3(22): 6783-6799.
[25] Shimpi R P, Patel H G. Free vibrations of plate using two variable refined plate theory. Journal of Sound Vibration 2006; 296(4-5): 979-999.
[26] Marur P R. Fracture behaviour of functionally graded materials. PhD thesis, Aubum University, 1999.
[27] Delale F, Erdogan F. The crack problem for a nonhomogeneous plane. Journal of Applied Mechanics 1983; 50(3): 609-614.
[28] Zenkour A M. Generalized shear deformation theory for bending analysis of functionally graded plates. Applied Mathematical Modelling 2006; 30(1): 67-84.
[29] Matsunaga H. Stress analysis of functionally graded plates subjected to thermal and mechanical loadings. Composite Structure 2009; 87(4): 344-357.

Biography:

Abdelouahed TOUNSI Born in 1971, he is a professor and doctoral supervisor in Sidi Bel Abbes University. His main research interest involves materials and structures.
E-mail: tou_abdel@yahoo.com